Dynamic elements of mixedmode oscillations and chaos in a peroxidase–oxidase model network

Baltazar D. Aguda, Raima Larter, and Bruce L. Clarke

Citation: The Journal of Chemical Physics **90**, 4168 (1989); doi: 10.1063/1.455774
View online: http://dx.doi.org/10.1063/1.455774
View Table of Contents: http://scitation.aip.org/content/aip/journal/jcp/90/8?ver=pdfcov
Published by the AIP Publishing

Dynamic elements of mixed-mode oscillations and chaos in a peroxidase–oxidase model network

Baltazar D. Aguda and Raima Larter
Department of Chemistry, Indiana University–Purdue University at Indianapolis, Indianapolis, Indiana 46205

Bruce L. Clarke
Department of Chemistry, University of Alberta, Edmonton, Alberta, Canada T6G 2G2

(Received 21 November 1988; accepted 27 December 1988)

Three dynamic elements, DE-1, DE-2, and DE-3, are identified for the four-species Olsen model of the peroxidase–oxidase reaction. DE-1 is the damped Lotka oscillator which tends to generate smaller amplitude oscillations. DE-2 is a switch responsible for the transitions between a small and a larger amplitude oscillation. DE-3 is the reversible flux of O_2 which dominates the dynamics of the full network while the concentrations of the intermediates are low. DE-1 is identified with the peroxidase catalytic cycle and DE-2 with a reaction involving compound III in the realistic mechanism. Numerical simulations on the route to chaos are presented for varying parameters affecting the three dynamic elements. Pictures of the evolution of the strange attractor that accompanies chaotic oscillations are given. As shown in the Poincaré sections of the attractor and Poincaré next-return maps, the layers of this attractor develop as even- and odd-period fixed points undergo cascades of period doubling.

I. INTRODUCTION

In a previous paper (Ref. 1), the origin of the chaotic oscillations exhibited by the Willamowski–Rössler model (Ref. 2) is discussed in terms of the components of the reaction network called *dynamic elements*. The numerical simulations demonstrated that the complex oscillations were mainly caused by the interaction of two dynamic elements: one is the Lotka–Volterra oscillator and the other is a switch between two competing autocatalytic species. In this paper, we use this approach of analyzing the structure of a reaction network to elucidate the source of the mixed mode as well as the chaotic oscillations shown by the Olsen model (Ref. 3). This model was proposed to simulate the complex dynamical behavior of the peroxidase–oxidase reaction observed in the laboratory.

Throughout this paper, we refer to the aerobic oxidation of nicotinamide adenine dinucleotide (NADH) catalyzed by the horseradish peroxidase enzyme as the *peroxidase–oxidase* reaction. The net overall reaction is

$$2\mathrm{NADH} + 2\mathrm{H}^+ + \mathrm{O}_2 \rightarrow 2\mathrm{NAD}^+ + 2\mathrm{H}_2\mathrm{O}. \qquad (1)$$

When carried out in an open system, this reaction exhibits a variety of dynamics including switching between two stable steady states (Refs. 4 and 5), damped (Ref. 6) and sustained oscillations (Refs. 3 and 4), and even chaos (Refs. 3 and 4). The mechanism for the reaction is widely believed to be a free radical branched chain mechanism (Refs. 7 and 8).

Using mostly the experimentally established elementary processes involved in the reaction, the origin of bistability has been accounted for (Ref. 9). In a simplified model extracted from this realistic mechanism (Ref. 9), it was assumed that NADH is in stoichiometric excess and is not considered a dynamical species. This simplified model exhibited bistability. [An analysis of a different peroxidase–oxidase model that also disregards NADH as a dynamical species (Ref. 10) likewise showed bistability.] The multiplicity of steady states (two stable, one unstable) was shown to be caused by a substrate-inhibition mechanism involving three elements: the peroxidase catalytic cycle, an inhibition cycle involving an enzyme intermediate called compound III and a reversible input of the substrate oxygen. These elements represent the minimum subset of the realistic mechanism that could generate three steady states. This minimum bistable model was also shown to generate damped oscillations (Ref. 9). The results of the analysis of Fed'kina and coworkers (Ref. 11) on a similar realistic model indicate strongly that this minimum bistable model will show sustained oscillations somewhere in parameter space.

A model mechanism for the sustained oscillations in the peroxidase–oxidase reaction was proposed by Degn, Olsen, and Perram (DOP) (Ref. 4). Later, Olsen (Ref. 3) proposed a slightly different model that displays the nonperiodic oscillations observed in experiments over a wider range of parameter values than the DOP model. The Olsen model is the subject of the present paper. Previous numerical simulations using the Olsen model have shown remarkable qualitative resemblance of the computed concentration-time plots to the experimentally determined data for the species NADH and O_2 (Refs. 4 and 8). Section II describes the Olsen model and its kinetic equations. Section III reports on the local stability of the steady states within the region of parameter space that gives complex oscillations. Section IV provides a discussion of the dynamic elements of the network and shows how the switching between small and large amplitude oscillations occur. Section V describes the route to chaos in this model and shows the evolution of the accompanying strange attractor.

II. OLSEN'S MODEL MECHANISM OF THE PEROXIDASE–OXIDASE REACTION

Olsen (Ref. 3) proposed the following mechanism to simulate the experimentally observed nonperiodic oscilla-

 0021-9606/89/084168-08$02.10

tions in the peroxidase–oxidase reaction:

$$\begin{aligned} B + X &\rightarrow 2X, && \text{(R1)}\\ 2X &\rightarrow 2Y, && \text{(R2)}\\ A + B + Y &\rightarrow 3X, && \text{(R3)}\\ X &\rightarrow ( ), && \text{(R4)}\\ Y &\rightarrow ( ), && \text{(R5)}\\ ( ) &\rightarrow X, && \text{(R6)}\\ ( ) &\rightleftarrows A, && \text{(R7)}\\ ( ) &\rightarrow B. && \text{(R8)} \end{aligned}$$

Species A is O_2 and species B is NADH. X and Y are important intermediates that are involved in the branched chain mechanism. The reversible reaction (R7) corresponds to the dissolution of gaseous oxygen into the aqueous phase. ( ) indicates either a constant reservoir of the corresponding species or a termination of the species into nonreactive products. Being a mathematical model, this mechanism condenses several elementary kinetic processes into steps which, when endowed with mass-action kinetics, capture the essential rate laws of those component processes.

The time evolution of the species concentrations under isothermal and homogenous conditions is summarized by the following system of autonomous ordinary differential equations (we use the same species symbols to denote concentrations):

$$\begin{aligned} \dot{A} &= k_7 - k_{-7}A - k_3ABY,\\ \dot{B} &= k_8 - k_1BX - k_3ABY,\\ \dot{X} &= k_1BX - 2k_2X^2 + 3k_3ABY - k_4X + k_6,\\ \dot{Y} &= 2k_2X^2 - k_5Y - k_3ABY. \end{aligned} \tag{2}$$

Figure 1 gives the network diagram for this model and shows the presence of two feedback loops both involving the species X and B. Analogies between these feedback loops in the model and those found in proposed realistic mechanisms can be made. One of the feedback loops in the Olsen model [reaction (R1)] corresponds to the peroxidase catalytic cycle which generates a large number of NAD· radicals. The other feedback loop involving the intermediate Y [reactions (R2) and (R3)] corresponds to the cycle involving the enzyme intermediate called compound III (Ref. 11). As shown in realistic mechanisms (Refs. 7 and 8), this latter cycle is less efficient than the first in generating NAD· radicals. Correspondingly, in the Olsen model, because of the exit reaction (R5) and the delay of the positive feedback on X (that is, by going through the intermediate Y before reproducing X) the second feedback loop is less efficient than the direct autocatalysis in reaction (R1).

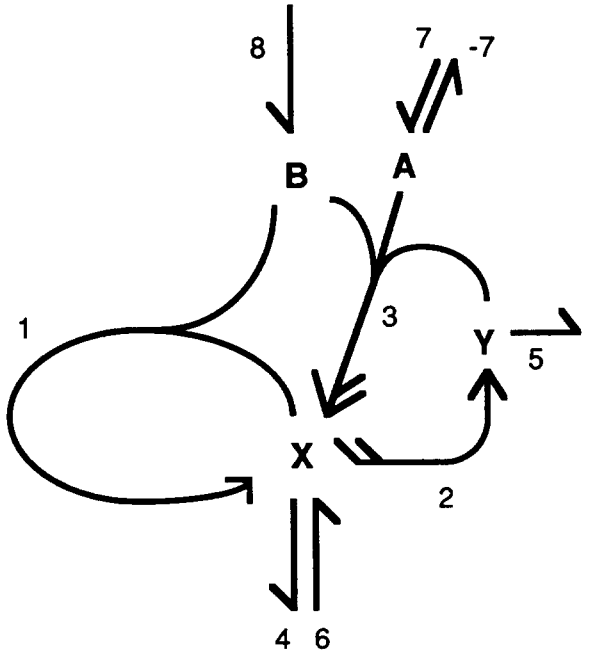

FIG. 1. Network diagram of the Olsen model of the peroxidase–oxidase reaction. Only the dynamical species are shown. There are two feedback loops: one involving reaction 1, and the other involving the combination of reactions 2 and 3. The number of barbs on the reaction arrows indicate the number of molecules of product formed. The number of feathers on the left side of the arrow tail indicate the order of kinetics with respect to the corresponding reactant. If the order of reaction is 1, no feather is drawn.

The Olsen model is similar to an earlier mechanism proposed by Degn, Olsen, and Perram (DOP) (Ref. 4). In contrast to the Olsen model, the DOP model includes species A as a reactant in reaction (R1), that is, $A + B + X \rightarrow 2X$ is (R1) in the DOP model. Including A in (R1) allows this step in the DOP model to be identified with the reaction between O_2 and NAD· producing a superoxide anion radical (O_2^-); the latter species eventually feeds into the peroxidase catalytic cycle (Refs. 7 and 8). The participation of species A in the trimolecular step (R3) in both the Olsen and DOP models is explained by the experimentally known reaction between oxygen and ferrous peroxidase (Refs. 7 and 8); this latter reaction enters the feedback loop involving compound III in the realistic mechanism. A model in which species A feeds only in the first feedback loop like (R1) in the DOP model but, unlike the Olsen model, has (R3) as $B + X \rightarrow 3X$, would also be consistent with the known mechanism of the peroxidase–oxidase reaction and warrants further investigation.

The Olsen and DOP models both produce simple and complex oscillations. Both models also produce chaos but the regions in parameter space that have been explored so far indicate that chaos is observed over a broad range of parameter values in the Olsen model (Ref. 3) and narrow ones in the DOP model (Ref. 10). Furthermore, a pruned Farey tree is found in the Olsen model (Ref. 3) while a more complete Farey tree is found in the DOP model (Ref. 12). We cannot, as yet, distinguish between these two models experimentally since complex periodic oscillations have not been observed in the laboratory.

III. THE STEADY STATES AND THEIR LOCAL STABILITY

Linear stability analysis of the steady states of dynamical systems can sometimes aid in the exploration of chaotic behavior. The difficulty in predicting bifurcations to chaotic behavior primarily lies in the global character of this phenomenon and linearization techniques usually do not apply. However, an encouraging result is the observation that many transitions which are global when one control parameter is varied become local when more than one such parameters are considered. Indeed, complex nonperiodic behavior has already been observed near certain codimension-two bifur-

cation points (Ref. 13). In this section, we provide the complete solution for the steady states of the Olsen model [Eq. (2)] as functions of the rate constants. The eigenvalues associated with the system linearized about these steady states are then calculated for a range of values of k_1, including those associated with nonperiodic oscillations.

The steady states of the Olsen model are found by setting the right-hand side of Eq. (2) to 0. The steady states of species Y, A, and B are found to be expressible in terms of the steady state of species X according to

$$Y_s = (2k_2X_s^2 + k_6 + k_8 - k_4X_s)/(2k_5), \quad (3)$$

$$A_s = (k_6 + k_7 + k_8 - k_4X_s - k_5Y_s)/k_{-7}, \quad (4)$$

$$B_s = (k_6 + 2k_8 - k_4X_s - k_5Y_s)/(k_1X_s), \quad (5)$$

where the subscript s signifies the steady state value. The steady state X_s is a positive root of the following sextic polynominal:

$$P_6(X_s) = \beta_6X_s^6 + \beta_5X_s^5 + \cdots + \beta_1X_s + \beta_0 = 0, \quad (6)$$

where

$$\beta_6 = 8k_3k_2^3,$$

$$\beta_5 = 4k_3k_4k_2^2,$$

$$\beta_4 = -2k_2k_3(6k_2k_8 + 4k_2k_7 + 2k_2k_6 + k_4^2),$$

$$\beta_3 = 4k_2k_3k_4(k_6 + k_8) - 8k_1k_2k_5k_{-7} - k_3k_4^3,$$

$$\beta_2 = 8k_2k_3k_7k_8 - 2k_2k_3k_8^2 - 4k_2k_3k_6k_8 - 2k_2k_3k_6^2 + 5k_3k_8k_4^2 + 2k_3k_7k_4^2 + 3k_3k_6k_4^2 - 4k_1k_4k_5k_{-7},$$

$$\beta_1 = 4k_1k_5k_{-7}(k_6 + k_8) - 7k_3k_4k_8^2 - 8k_3k_4k_7k_8 - 10k_3k_4k_6k_8 - 4k_3k_4k_6k_7 - 3k_3k_4k_6^2,$$

$$\beta_0 = k_3(3k_8^3 + 6k_7k_8^2 + 7k_6k_8^2 + 8k_6k_7k_8 + 5k_8k_6^2 + 2k_7k_6^2 + k_6^3).$$

Equations (3)–(5) give the relationships between the steady states of all the species. The relationship between Y_s and X_s given by Eq. (3) is parabolic; Y_s first decreases from the value $(k_6 + k_8)/(2k_5)$ as X_s increases from 0 and after reaching a minimum, Y_s increases parabolically as a function of X_s. The steady state of species A decreases as X_s or Y_s increases. The constraints $Y_s > 0$, $A_s > 0$, and $B_s > 0$ should be used to determine the positive roots of Eq. (6) that are allowed.

The eigenvalues of the Jacobian of Eq. (2) evaluated at the steady state values given by Eqs. (3)–(5) are shown in Fig. 2 as a function of k_1. We found only one steady state over the parameter range shown in this figure. Below the eigenvalues, we show the corresponding time-dependent behavior; some of this information was previously reported by Olsen (Ref. 3). A Hopf bifurcation is found at a value of $k_1 = 1.466$ (values of the other parameters given in Fig. 2). No codimension-two bifurcation point involving a pair of complex conjugate eigenvalues and one real eigenvalue crossing the imaginary axis simultaneously was found. At $k_1 = 0.3491$, a pair of complex conjugate eigenvalues with

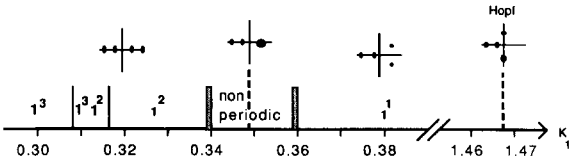

FIG. 2. Periodic states and Argand diagrams of the four eigenvalues associated with the unique steady state of the Olsen model as k_1 is varied. Values of other rate constants are $k_2 = 250$, $k_3 = 0.035$, $k_4 = 20$, $k_5 = 5.35$, $k_6 = 10^{-5}$, $k_7 = 0.8$, $k_{-7} = 0.1$, $k_8 = 0.825$. The dots indicate the position of the eigenvalues with respect to the real and imaginary axes. The large dot at $k_1 = 0.3491$ indicates two identical real eigenvalues. Hopf bifurcation occurs at $k_1 = 1.466$. The notation L^s indicates L large and s small amplitude limit cycle oscillations. The shaded bars delineating the nonperiodic region indicate regimes of rapid period doublings of the oscillations.

positive real parts fuse (become identical) at the real axis as k_1 is decreased. A further decrease of k_1 will then separate these identical eigenvalues into two real positive eigenvalues. In other words, at the parameter point where the identical eigenvalues occur the derivative of both the real and imaginary parts of these eigenvalues vanish. It is interesting to note that this occurs in the middle of the region where chaos is observed in the numerical simulations; we currently have no explanation for this behavior.

IV. SWITCHING BETWEEN DYNAMIC ELEMENTS LEADING TO MIXED-MODE OSCILLATIONS

A first step in understanding the behavior of the Olsen model is to analyze the dynamics of the feedback loops involving only the intermediates X and Y (keeping the other species at constant concentrations). Because of the autocatalytic nature of the two feedback loops, X and Y can explode stoichiometrically. However, the introduction of a single flow term could turn this explosion into extinction: for example, the subnetwork composed of the (pseudo-)reactions (R1), $(X \rightarrow 2X)$ and (R4), $(X \rightarrow)$ will show extinction of X if $k_4 > k_1$. In the full Olsen model, the explosions and extinctions are regulated by the flow terms involving the major dynamical species A and B [as well as the exit reactions (R4) and (R5)].

The excitability of the system is shown by the plots of X vs. time and Y vs. time in Fig. 3. When the intermediates X and Y have very low concentrations, A and B accumulate and after reaching some critical concentrations, similar to a critical mass of a water droplet in a dripping faucet (Ref. 14), the system suddenly gives way to oscillations as A and B are emptied. This emptying phenomenon can be seen in the A vs. time and B vs time plots of Fig. 3.

In order to acquire a further understanding of the dynamics of the Olsen model, we have determined which steps in the reaction network are dominant as the system goes through large and small amplitude oscillations. Figure 4 shows a typical limit cycle composed of one small and one large amplitude oscillation. We have labeled six segments along this limit cycle at which we have identified the dominant reactions. At **a**, the large increase in X is brought about mostly by the autocatalytic reaction (R1). X increases to a sufficient level that speeds up the second-order reaction (R2). Therefore at **b**, Y increases, X decreases and reaction

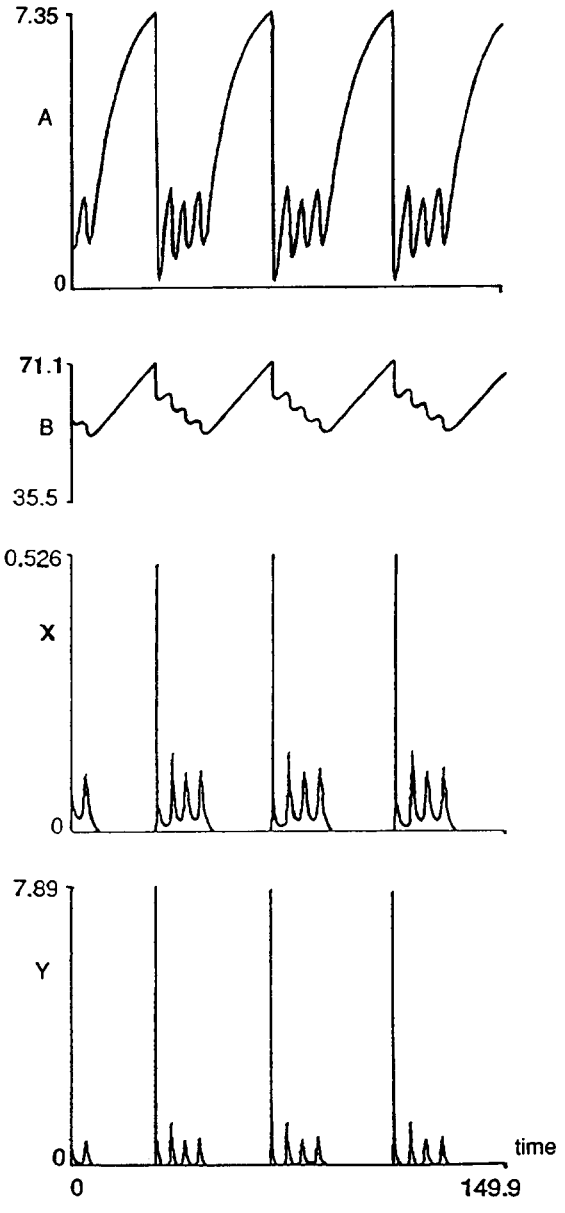

FIG. 3. Concentration-time plots of the four dynamical species of the Olsen model. Parameter values as in Fig. 2 except $k_1 = 0.30$. All integrations in this paper used the GEAR algorithm (Ref. 17). Initial conditions: $A_0 = 1.161$, $B_0 = 56.41$, $X_0 = 0.086\,57$, and $Y_0 = 0.5727$.

(R3) speeds up thereby decreasing B. At **c**, X is increasing again due to reaction (R3) but not to a level that would hasten reaction (R2) again; instead, the first-order reaction (R4) consumes X as shown in **d**. B and X are not high enough at this time to make the speed of reaction (R1) appreciable. But at **e**, X begins to increase again through reaction (R1) although the level of B is not as high as before (in **a**). The amplitude is smaller now because the speed of reaction (R1) is slower. In **f**, reaction (R2) is slower than reaction (R4) and hence Y does not increase as much as before (in **b**). Then X decreases again. Note that if X has decreased to a very low value, B has the chance to accumulate and the large amplitude oscillation is started again due to the rapid increase in X through reactions (R1) and (R3).

We also see from Fig. 4 and the observations above that the value of Y is critical in the switching between a large and

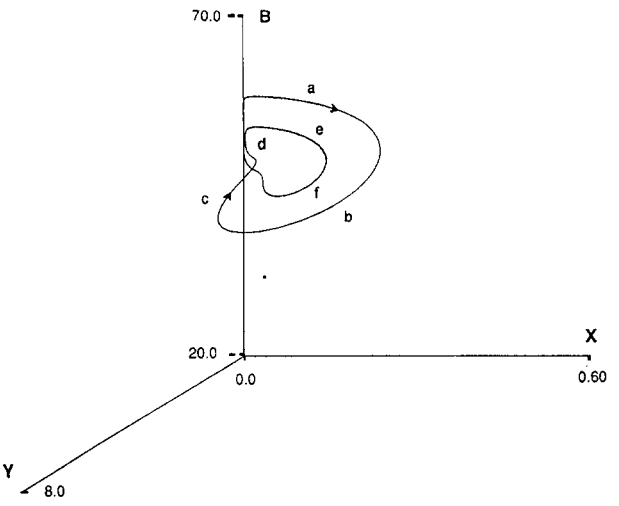

FIG. 4. A mixed-mode limit cycle (one large and one small amplitude oscillation) generated by the Olsen model. The square dot below the limit cycle gives the position of the calculated unique steady state. Parameter values are the same as in Fig. 2 except $k_1 = 0.37$.

a small amplitude oscillation. In a large amplitude oscillation, the large increase in X leads to a large increase in Y through the second-order reaction (R2). A high level of Y will cause the depletion of B through reaction (R3). This decrease in B will strongly retard the production of X since B affects both the speed of reactions (R1) and (R3) which are the reactions producing X. A low level of B gives rise to a small amplitude oscillation.

The next step in understanding the dynamics of the full Olsen model is to determine whether it is possible to identify subsets of the network (or subnetworks) that could dominate the dynamics of the full network at different time intervals. When this is the case, some reactions will act as switches between these subnetworks. A common switch is the reaction between species W and V shown in Fig. 5. If W and V are produced at the same rate [$k_2 = k_3$ in Fig. 5(a)], then there is a continuum of marginally stable steady states where the nullclines $\dot{W} = 0$ and $\dot{V} = 0$ coincide. When the rates of production of the competing species are not equal, the species that is being produced faster will explode while the other gets depleted. As in the case shown in Fig. 5(b), the nullclines no longer coincide. We refer to these subnetworks just

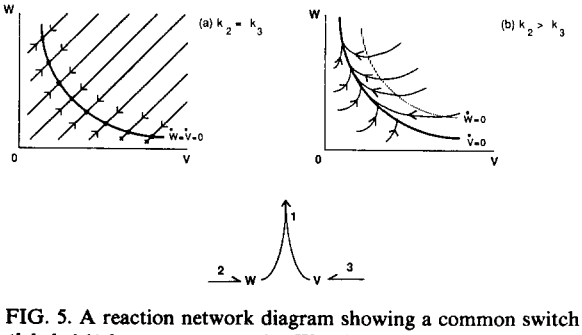

FIG. 5. A reaction network diagram showing a common switch reaction (labeled 1) between two species W and V. The network shown has an infinite number of marginally stable steady states if the two competing species are produced at the same rate [shown in (a)]; otherwise one of the species explodes and the other becomes extinct [shown in (b)].

described and their switching reactions as the *dynamic elements* of a network.

We now propose that one of the dynamic elements in the Olsen model is the subnetwork composed of reactions (R8), (R1), (R4), and (R6) (see Fig. 1). In fact, this subnetwork is the Lotka damped oscillator (Ref. 15). We shall refer to this dynamic element as DE-1. It is known to exhibit damped oscillations under certain parameter values (for example, when $k_8 = 0.825$, $k_1 = 0.35$, $k_4 = 20$, and $k_6 = 10^{-5}$; other rate constants are 0). Sustained oscillations cannot be generated by DE-1 alone. When we mix a small amount of the second feedback loop of the Olsen model (obtained by setting $k_2 = 1.0$, $k_3 = 0.01$, $k_5 = 5.35$, $k_7 = 0.8$, and $k_{-7} = 0.1$) with DE-1 (with the rate constants k_8, k_1, k_4, and k_6 as given above), one finds that the full network can give oscillations that are sustained (a limit cycle). The reason for this is the rapid production of X by the second feedback loop once the concentrations of Y, A, and B have reached sufficiently high levels. This counteracts the damping tendency of DE-1.

Fed'kina and co-workers (Ref. 11) have concluded from their simulations based on a realistic mechanism that only damped oscillations can be generated by the system if compound III is missing. This is further supported by our later work (Ref. 9) that showed oscillations towards a steady state in which the peroxidase catalytic cycle is much more dominant than the inhibition cycle involving compound III. We propose, on the basis of these observations, that species Y is analogous to compound III in the realistic mechanism.

As we have seen earlier in this section, reaction (R3) enables the switching between small and large amplitude oscillations. This switching reaction is triggered by a spike in the level of Y following a spike in X (see Fig. 3). Because Y is being produced faster than B and A when this spike occurs, reaction (R3) tends to deplete A and B. Reaction (R1) slows down because of the decrease in B and the concentrations of X and Y will then decrease because of reactions (R4) and (R5), respectively. These low levels of X and Y will now allow A and B to accumulate back and start a large amplitude oscillation all over again. We will refer to reaction (R3) as the switch dynamic element, DE-2.

From the plot of A vs. time in Fig. 3 we see that the reversible reaction (R7) is not perturbed by reaction (R3) and A increases parabolically towards a value of k_7/k_{-7} as long as Y is small. Because for a significant time interval the dynamics of the full network is dominated by the reversible reaction (R7), we consider this equilibrium reaction as another dynamic element and will refer to it as DE-3 subsequently.

V. CHAOTIC OSCILLATIONS AND THE ACCOMPANYING STRANGE ATTRACTOR

Olsen (Ref. 3) has reported the existence of chaos and the accompanying strange attractor in numerical simulations of this model. Similar results have been found in experimental data for the peroxidase–oxidase reaction (Ref. 3). In this section, we report additional numerical studies which are designed to illuminate the source of the nonperiodic oscillations exhibited by the model over a wide range of parameter space. Reactions (R1) and (R2) affect the dynamic elements DE-1 and DE-2, respectively, and therefore we explored the dynamics by varying the rate constants k_1 and k_2 near those values that give nonperiodic oscillations. Furthermore, the effect of the third dynamic element, DE-3, on the evolution of the strange attractor is studied by varying k_{-7}.

A. Increasing the damping effect of DE-1

Because of the correspondence between experimental variation of enzyme concentration and mathematical variation of the value of k_1, Olsen (Ref. 3) considered k_1 to be proportional to the enzyme concentration. A dynamical interpretation is that varying k_1 lets us control the damping of the oscillations of the full network by the Lotka element (DE-1). The magnitude of the damping is directly related to the magnitude of the negative real part of the eigenvalues of the Jacobian matrix evaluated at the steady state. For DE-1, under damped oscillatory conditions, the real part of the eigenvalues, $\mathrm{Re}(\lambda)$, has a magnitude that increases linearly with k_1 as follows:

$$\mathrm{Re}(\lambda) = \frac{-k_1(k_6 + k_8)}{2k_4} - \frac{k_4}{2} + \frac{k_4 k_8}{2(k_6 + k_8)}. \qquad (7)$$

Thus, as k_1 is increased we expect that the amplitude of the oscillations of the full network should decrease. This is indeed the case as shown in Fig. 6.

Figure 6 shows three-dimensional plots of the oscillations in B-X-Y concentration space. All plots except Fig. 6(d) show the stable limit cycles which exist for different

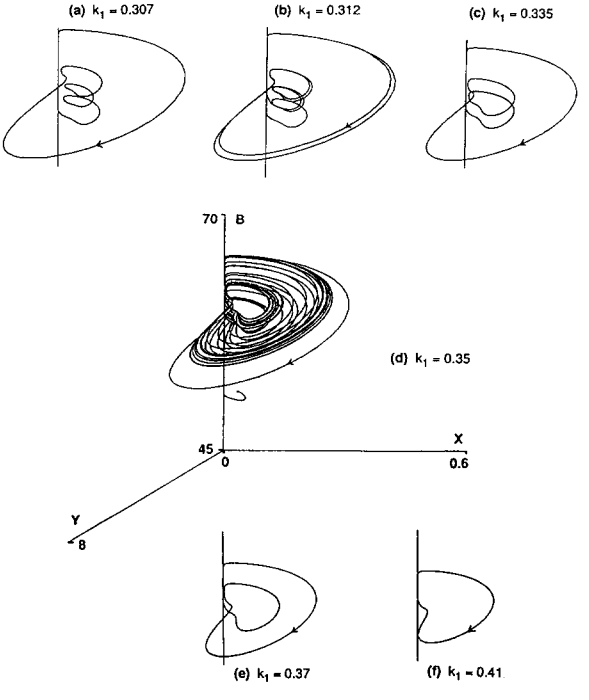

FIG. 6. Three-dimensional plots of the oscillations in B-X-Y space as k_1 is varied. Except (d), all transients are discarded and all oscillations shown are limit cycles. In (d), the trajectory is started near the steady state (the dot) and the resulting oscillations are nonperiodic. The vertical lines in (a)–(c) and (e)–(f) are part of the B axis. (All parameter values are the same as in Fig. 2 except k_1).

values of k_1; all transients have been discarded. In Fig. 6(d), the trajectory was started very close to the computed steady state indicated by a dot; the trajectory is attracted to a region where nonperiodic oscillations occur. The sequence of oscillatory states were previously reported by Olsen (Ref. 3). A cascade of period doubling bifurcations occurs from both sides of the nonperiodic region. (See also Fig. 2.)

As shown in Fig. 2, over a range of k_1 values from 0.309 to 0.316 limit cycle oscillations are observed which have the form $1^3 1^2$, i.e., concatenation of the 1^3 (1 large, 3 small amplitude) and the 1^2 (1 large, 2 small amplitude) oscillations found immediately outside this region. The concatenation of the corresponding trajectories in phase space is clearly shown in Figs. 6(a)–6(c). In Fig. 6(b), there is a region in concentration space where the trajectories strongly diverge in two directions; when the trajectory goes in one direction, the result is a 1^2 oscillation while the movement in the other direction results in a 1^3 oscillation. We did not find a devil's staircase in the Olsen model that was as nearly complete as the one we found in the DOP model (Ref. 12). We again observe in the three-dimensional plots in Fig. 6 how the level of B affects the amplitude of the oscillation and creates the finer structure of the chaotic attractor.

B. Effect of varying k_2 on DE-2

Increasing k_2 will increase the net rate of production of Y which, as we have seen in Sec. IV, is important in the switching between small and large amplitude oscillations. Figure 7 shows some plots of trajectories in B-X-Y concentration space obtained by varying k_2. In all plots all transients were discarded. In Fig. 7(a), single amplitude limit cycle oscillations are found which then undergo a series of period-doubling bifurcations, one of which is shown in Fig. 7(b). Further period doublings result in nonperiodic (infinite period) oscillations shown partly in Fig. 7(c). Beyond the values of k_2 that give nonperiodic oscillations, a three-loop oscillation (1^2) is found. These observations on both sides of the nonperiodic region are qualitatively the same as what we have seen when we varied k_1 but in reverse order; increasing k_1 results in a sequence of transitions that can be reproduced by decreasing k_2. This result is expected because increasing k_2 and decreasing k_1 have the same effect of decreasing the rate of production of X.

C. Effect of DE-3

The net production of A due to the reversible reaction (R7) (DE-3) affects the switch DE-2 as discussed above. Increasing k_{-7} (at constant value of k_7) will decrease the net production of A and, from the viewpoint of competing species A and Y in (R3), will have the equivalent effect of increasing k_2. This is confirmed by the Poincaré sections given in the discussion below.

D. Evolution of the strange attractor

Figure 8 shows a nonperiodic oscillation (started from a single initial condition) on the X-Y plane. All initial conditions on this plane will eventually be pulled towards the attractor shown in this figure. If a line is drawn across the attractor as shown in Fig. 8, and a plot is made of the next-return map (an intersection point of the trajectory with the line versus the next intersection point), a map similar to what is shown in Fig. 9(c) is obtained. It is equivalent to the next-amplitude map that was first reported by Olsen (Ref.

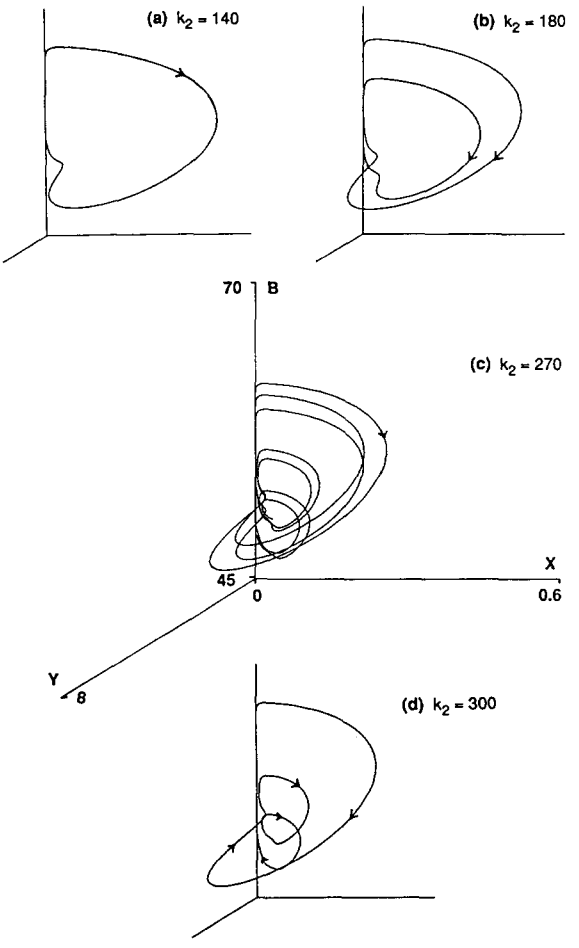

FIG. 7. Three-dimensional plots of the oscillations in B-X-Y space as k_2 is varied. Except (c), all transients are discarded and all oscillations shown are limit cycles. In (c), the trajectory is started near the steady state (the dot) and the resulting oscillations are nonperiodic. (All parameter values are the same as in Fig. 2 except k_2 and $k_1 = 0.35$).

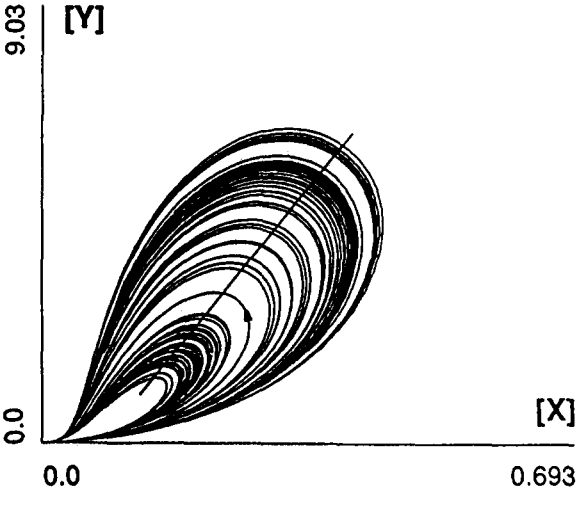

FIG. 8. Projection of the nonperiodic trajectories on the X-Y plane. All transients have been discarded. The line segment is used to generate Poincaré next-return maps and sections of the strange attractor as described in the text. (All parameters are the same as in Fig. 2 except $k_1 = 0.35$.)

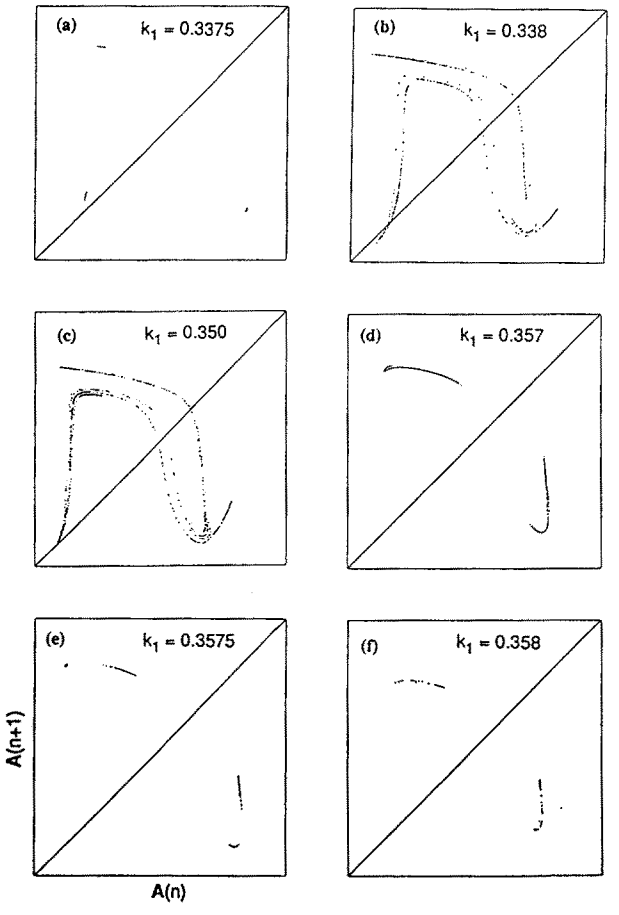

FIG. 9. Evolution of the strange attractor as k_1 is varied. (All parameters as in Fig. 2 except k_1.) The Poincaré next-return maps plot the concentration of species A; $A(n)$, versus its next-return value, $A(n+1)$, on a certain Poincaré line segment similar to the one shown in Fig. 8 (the line segment in this case will be cutting through the attractor on the A-X plane).

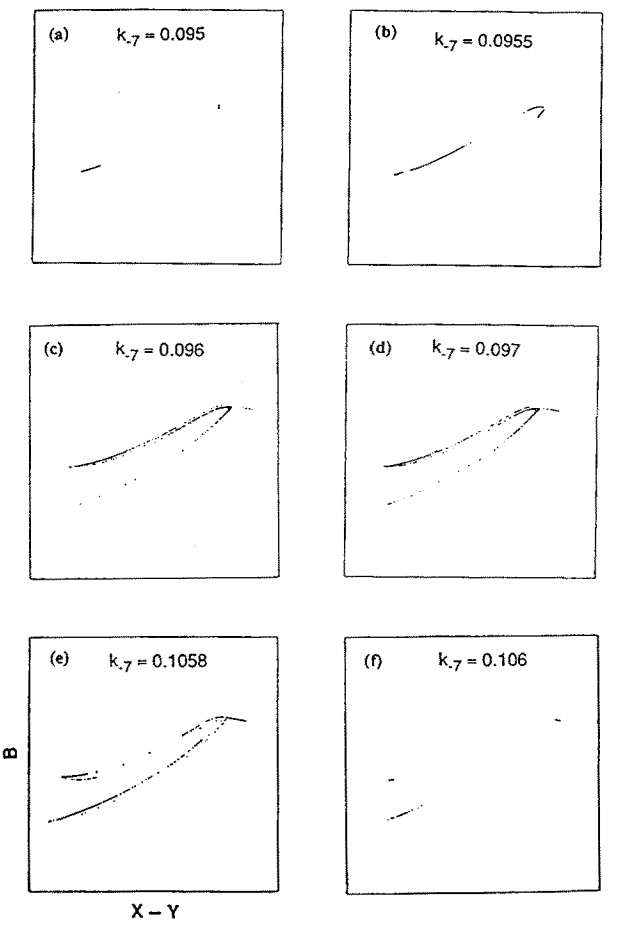

FIG. 10. Evolution of the strange attractor as k_{-7} is varied. (All parameters are the same as in Fig. 2 except k_{-7} and $k_1 = 0.35$.) The Poincaré sections shown plot the intersection points between the trajectories on the attractor in B-X-Y three-dimensional space and the plane perpendicular to the X-Y plane and directed towards the positive B direction. The abscissa labeled X-Y refer to the line segment shown in Fig. 8.

3). Olsen has also given evidence of the fractal nature of this strange attractor.

A three-dimensional picture of the strange attractor can be ascertained by taking Poincaré sections. If one cuts the strange attractor along a plane that is perpendicular to the X-Y plane, directed towards the positive B axis and with the width indicated by the line segment shown in Fig. 8, then one gets a Poincaré section similar to what is shown in Fig. 10(d). The Poincaré sections are topologically equivalent to the next-return maps (Ref. 16).

How the complicated structure of the strange attractor develops can be gleaned from the pictures provided in Figs. 9 and 10. In Fig. 9, the series of pictures with decreasing k_1 [Figs. 9(f) → 9(e) → 9(d)] corresponds to a cascade of period doubling bifurcations of the fixed points of even periods. In Fig. 10, where the Poincaré sections of the chaotic attractor are shown, the corresponding series would be the increasing values of k_{-7} [Figs. 10(a) → 10(b)]. In both figures, the resulting fixed points (with even periods) tend to lie on some well-defined curves. The fixed points with odd periods (starting from period 3) also undergo a cascade of period doubling and the resulting fixed points lie on some identifiable curves as shown in Fig. 9 [Figs. 9(a) → 9(b)] and Fig. 10 [Figs. 10(f) → 10(e)]. The manifolds of even-period fixed points and odd-period fixed points then entangle at the parameter values where the strange attractor is fully developed, that is, in Fig. 9(c) and in Fig. 10(d).

VI. CONCLUDING REMARKS

We have identified three dynamic elements of the Olsen model for the peroxidase–oxidase reaction. DE-1 is the damped Lotka oscillator involving a direct autocatalysis of the intermediate species X. DE-1 tends to pull trajectories towards the steady state and is thus responsible for the smaller amplitude oscillations exhibited by the full system. DE-2 is a switch reaction responsible for the transitions between a small and a larger amplitude oscillation. We have also seen that the intermediate Y is important in sustaining the oscillations as well as triggering the switch DE-2. The third dynamic element, DE-3, involves species A in a reversible reaction which is almost undisturbed by the other reactions until the switch DE-2 becomes significant.

We have demonstrated the influence of the three dynamic elements DE-1, DE-2, and DE-3 on the nature of the complex periodic oscillations in the Olsen model. The essential feature of these oscillations, which is a switching between a large amplitude cycle and a small amplitude cycle, can be understood in terms of the dynamic element DE-2

switching the flow from the subnetwork DE-1 to the subnetwork DE-3. When conditions are such that chaotic behavior is displayed by this mechanism, this switching occurs at random and intermediate-amplitude oscillations become more and more common. Mechanistically, it is not yet clear to us why the time interval at which switching occurs is unpredictable under these conditions.

We have presented detailed pictures of the evolution of the chaotic attractor through the Poincaré next-return maps in Fig. 9 and the topologically equivalent Poincaré sections in Fig. 10. Looking at how the manifolds of even- and odd-period fixed points (through period doubling) develop it becomes clear that the layers of the strange attractor are due to the interlacing of these manifolds. Future analytic calculations on this model to determine the mathematical nature of the dynamical bifurcations will be aided by these pictures.

Lastly, we confirm the validity of the Olsen model as a model to simulate the complex dynamics of the peroxidase–oxidase reaction in an open system. Comparing the results on the analysis of this model and analyses of more realistic mechanisms of the reaction, the following analogies can be made: the first feedback loop of the Olsen model corresponds to the peroxidase catalytic cycle, and the second feedback loop of the Olsen model corresponds to the cycle involving compound III. The dynamical roles of species X and Y in the Olsen model are analogous to those of species $NAD^{\cdot}$ and compound III, respectively, in the realistic mechanism.

ACKNOWLEDGMENT

We gratefully acknowledge support of this work by the National Science Foundation under Grant No. CHE-8808191.

[1]B. D. Aguda and B. L. Clarke, J. Chem. Phys. **89**, 7428 (1988).
[2]K. -D. Willamowski and O. E. Rössler, Z. Naturforsch. **35A**, 317 (1980).
[3]L. F. Olsen, Phys. Lett. **A94**, 454 (1983).
[4]H. Degn, L. Olsen, and J. Perram, Ann. N. Y. Acad. Sci. **316**, 623 (1979).
[5]H. Degn, Nature **217**, 1047 (1968).
[6]I. Yamazaki, K. Yokota, and R. Nakajima, Biochem. Biophys. Res. Commun. **21**, 582 (1965).
[7]K. Yokota and I. Yamazaki, Biochem. **16**, 1913 (1977).
[8]L. F. Olsen and H. Degn, Biochim. Biophys. Acta **523**, 321 (1978).
[9]B. D. Aguda and B. L. Clarke, J. Chem. Phys. **87**, 3461 (1987).
[10]R. Larter, C. Steinmetz, and B. D. Aguda, J. Chem. Phys. **89**, 6506 (1988).
[11]V. R. Fed'kina, F. I. Ataullakhanov, and T. I. Bronnikova, Biophys. Chem. **19**, 259 (1984).
[12]R. Larter, C. L. Bush, T. R. Lonis, and B. D. Aguda, J. Chem. Phys. **87**, 5765 (1987).
[13]C. Baesens and G. Nicolis, Z. Phys. B **52**, 345 (1983).
[14]I. Yamazaki and K. Yokota, in *Biological and Biochemical Oscillators*, edited by B. Chance *et al.* (Academic, New York, 1973), pp. 109–114.
[15]A. Lotka, J. Phys. Chem. **14**, 271 (1910).
[16]N. H. Packard, J. P. Crutchfield, J. D. Farmer, and R. S. Shaw, Phys. Rev. Lett. **45**, 712 (1980).
[17]A. C. Hindmarsh, GEAR: Ordinary Differential Equation Systems Solver, UICD-30001 Rev. 3, Lawrence Livermore Laboratory 1974.